

Prediction of Classical Fracture Initiation Toughness

V. GENSHEIMER DEGIORGI, G. C. KIRBY III AND M. I. JOLLES

*Mechanics of Materials Branch
Materials Science and Technology Division*

November 11, 1988

AD-A201 636

DTIC
ELECTE
DEC 09 1988
S D
C
H

88 12 9 033

REPORT DOCUMENTATION PAGE				Form Approved OMB No 0704-0188	
1a REPORT SECURITY CLASSIFICATION UNCLASSIFIED			1b RESTRICTIVE MARKINGS		
2a SECURITY CLASSIFICATION AUTHORITY			3 DISTRIBUTION / AVAILABILITY OF REPORT Approved for public release; distribution unlimited.		
2b DECLASSIFICATION / DOWNGRADING SCHEDULE					
4 PERFORMING ORGANIZATION REPORT NUMBER(S) NRL Memorandum Report 6141			5 MONITORING ORGANIZATION REPORT NUMBER(S)		
6a NAME OF PERFORMING ORGANIZATION Naval Research Laboratory		6b OFFICE SYMBOL (if applicable) Code 6382	7a NAME OF MONITORING ORGANIZATION		
6c ADDRESS (City, State, and ZIP Code) Washington, DC 20375-5000			7b ADDRESS (City, State, and ZIP Code)		
8a NAME OF FUNDING / SPONSORING ORGANIZATION Office of Naval Research		8b OFFICE SYMBOL (if applicable)	9 PROCUREMENT INSTRUMENT IDENTIFICATION NUMBER		
8c ADDRESS (City, State, and ZIP Code) Arlington, VA 22217			10 SOURCE OF FUNDING NUMBERS	PROGRAM ELEMENT NO 61153N22	PROJECT NO RR022-0148
			TASK NO	WORK UNIT ACCESSION NO DN480-509	
11 TITLE (Include Security Classification) Prediction of Classical Fracture Initiation Toughness					
12 PERSONAL AUTHOR(S) DeGiorgi, V.G., Kirby, G.C., III and Jolles, M.I.					
13a TYPE OF REPORT Interim		13b TIME COVERED FROM _____ TO _____	14 DATE OF REPORT (Year, Month, Day) 1988 November 11		15 PAGE COUNT 23
16 SUPPLEMENTARY NOTATION					
17 COSATI CODES			18 SUBJECT TERMS (Continue on reverse if necessary and identify by block number)		
FIELD	GROUP	SUB-GROUP	Fracture / Initiation	Constitutive Strain energy,	Damage criteria. (JES)
19 ABSTRACT (Continue on reverse if necessary and identify by block number) Initiation of crack growth in ductile materials has long been a concern to the manufacturing and design community. The current analysis considers a definition of fracture at the continuum scale to determine the onset of fracture. The strain energy density associated with fracture at the continuum scale is used as the fracture criterion. The critical strain energy density and the scale invariant continuum stress-strain curve were determined from a hybrid computational-experimental analysis of the deformation of a series of tensile tests performed on cylindrical specimens of HY-100 steel. Computational simulation of fracture initiation in a compact specimen of HY-100 steel containing a crack was performed using two- and three-dimensional nonlinear finite element techniques and continuum toughness concepts. Predicted values of classical fracture toughness parameters are within 3.5 percent of experimentally determined values.					
20 DISTRIBUTION / AVAILABILITY OF ABSTRACT <input checked="" type="checkbox"/> UNCLASSIFIED/UNLIMITED <input type="checkbox"/> SAME AS RPT <input type="checkbox"/> DTIC USERS			21 ABSTRACT SECURITY CLASSIFICATION UNCLASSIFIED		
22a NAME OF RESPONSIBLE INDIVIDUAL V. Gensheimer DeGiorgi			22b TELEPHONE (Include Area Code) (202) 767-9027	22c OFFICE SYMBOL Code 6382	

CONTENTS

INTRODUCTION	1
CONTINUUM MATERIAL TOUGHNESS CONCEPTS	2
MATERIAL CHARACTERIZATION	3
FRACTURE INITIATION EXPERIMENT	4
FRATURE INITIATION SIMULATION	5
PREDICTION OF FRACTURE TOUGHNESS	7
SUMMARY	7
ACKNOWLEDGEMENTS	8
REFERENCES	8



Accession For	
NTIS GRA&I	<input checked="" type="checkbox"/>
DTIC TAB	<input type="checkbox"/>
Unannounced	<input type="checkbox"/>
Justification	
By _____	
Distribution/	
Availability Codes	
Dist	Avail and/or Special
A-1	

PREDICTION OF CLASSICAL FRACTURE INITIATION TOUGHNESS

INTRODUCTION

Linear elastic fracture theories have been used successfully to predict brittle fractures. However, brittle failures represent only a small portion of failures due to the presence of a crack. High toughness materials may exhibit large amounts of local deformation prior to fracture. In order to accurately predict failure in high toughness materials, damage and fracture theories which address ductile behavior are required.

Many failure criteria have been proposed for ductile materials. Predominant among the failure criteria proposed are contour integrals such as J [1] and crack tip opening displacement [2]. Some early work in the determination of ductile failure criteria consisted of use of correction factors to extend the region of applicability of linear elastic fracture mechanics by representing the effects of plasticity around the crack tip [3,4]. However, only a limited amount of plasticity can be approximated by such correction factors. In other instances linear elastic material damage and fracture criterion evolved into ductile criterion through enhancements which broadened the range of applicability of the failure criterion. The resistance curve analysis method is one such evolved damage and fracture criterion. Initial resistance curve analyses were based on a plasticity corrected stress intensity factor [5]. Resistance curve concepts were then extended to the case of limited plasticity and perfectly plastic material response with the incorporation of J as the failure criterion as shown permissible by Landes and Begley [6]. Additional work concentrated on developing J for conditions of full plasticity extending for a relatively large area around the crack tip [7,8]. With each stage of its development, the resistance curve concept has been extended in an effort to account for increased material ductility.

In general, when there is a relatively small amount of plasticity around the crack tip, failure criteria based on linear elastic concepts can be used successfully. However, in instances where large amounts of plasticity occur prior to failure, analysis methods based on linear elastic concepts are no longer capable of approximating the state of stress and strain near the crack tip. In order to accurately represent the state of stress and strain near the crack tip the analysis method and failure criteria used should explicitly include large deformation constitutive response.

The explicit consideration of ductile material behavior prior to fracture does not in and of itself alleviate all limitations which may be associated with a particular fracture mechanics analysis technique. Present day fracture mechanics analysis techniques have limitations which must be taken into consideration [9]. Limitations common to fracture mechanics analysis techniques include the mathematical prediction of physically unattainable conditions such as the existence of a stress, strain and strain energy density singularity, correct material characterization and the appropriateness of the chosen fracture criterion. The material characterization used for ductile fracture should include an accurate description of large strain response. The failure criterion for ductile fracture should not be limited by the amount of local deformation which occurs prior to fracture. Other areas of concern which may exist for specific problems include availability of suitable data to adequately characterize material deformation, effects of loading rate and history, interpretations of material data scatter and defect characterization.

In addition to the various limitations listed above, a feature common to many fracture criteria is the assumption that failure occurs at a dominant crack or defect which is observed or assumed to exist in the structure. Since failure is assumed to occur at a crack or a defect, these features must be present in the test specimen used to determine the critical values of the parameters in the fracture criterion.

A material damage and failure criterion which explicitly addresses ductile behavior can be developed based on a general continuum approach which utilizes the constitutive relations to describe deformation, damage and fracture by the continuous point variables of stress, strain and energy density. Continuum material toughness [10] is one such material damage and fracture criterion which is based on a general continuum approach and is the criterion used in the current analysis. For a structural analysis, the geometry and boundary conditions which define the problem and the constitutive relations representing the material are used in a computational solution for the stress, strain and energy density fields. The critical locations in the structure are identified from the computational simulation and the load or time to failure is determined from the local stress, strain and energy density histories. No a priori assumption as to the location or mode of failure is required. The failure criterion used is the strain energy density required to produce material fracture at the continuum scale. The use of an energy density as a failure criterion is consistent with the concepts presented by Freudenthal [11] on material behavior and scaling considerations. Previous work by Gillemot [12] used analytical and empirical techniques to determine the strain energy density per unit volume at fracture for cylindrical tensile specimens. The strain energy per unit volume absorbed by the material up to the instant of fracture was calculated from global specimen response and deformation geometry. In separate studies Matic et al [13] have used computational simulation along with the experimentally determined point of failure to determine the critical strain energy density. Calculations of critical strain energy density values from computational simulations are able to address large deformation continuum toughness in a manner appropriate for structural integrity analyses. Applications to structural integrity prediction which demonstrate the feasibility of continuum material toughness as a failure criterion include investigations by Matic and Jolles [14,15] into the defect tolerance of welded components and the role of material geometry and applied load on weld system performance.

In order to demonstrate the fundamental nature of continuum material fracture toughness as a material damage and fracture criterion, a computational simulation of ductile fracture initiation in a compact specimen of HY-100 steel under monotonic loading is performed. Results from a fracture initiation experiment are available for comparison. Continuum material toughness concepts are reviewed in order to clarify for the reader the choice and implementation of material fracture toughness at the continuum scale as a failure criterion. The critical strain energy density required for fracture at the continuum scale and the scale invariant continuum stress-strain relation are determined by appropriate analysis of data obtained from a series of cylindrical tensile specimens of the same material as the compact specimen. The continuum stress-strain relation is determined from hybrid computational-experimental analyses which include large strain response. Nonlinear finite element methods are used for the computational analyses.

CONTINUUM MATERIAL TOUGHNESS CONCEPTS

A continuum volume of material undergoing deformation is characterized by its multiaxial stress and strain state, σ_{ij} and ϵ_{ij} , respectively. For ductile metals, and other materials which exhibit inelastic deformation, the strain state is a function of the stress history as well as the stress state. The state of stress and strain may be related by a constitutive formulation which defines the strain increment $d\epsilon_{ij}$ from the current stress state.

The strain energy per unit mass at a given instant during deformation is:

$$w = \lim_{\Delta V \rightarrow 0} \frac{1}{\rho} \frac{\Delta W}{\Delta V} \quad (1)$$

$$= \int_0^{\epsilon_v} \frac{\sigma_{ij}}{\rho} d\epsilon_{ij} \quad (2)$$

where ρ is the mass density. The energy density incorporates both stress and strain into a fundamental quantity relevant to thermodynamic description of material deformation and damage. The energy density is a scalar quantity which takes into account all components of the stress and strain tensors in a physically consistent manner. Failure of the material, at the continuum scale, can be associated with the value of the energy density at which fracture occurs. Thus, the material toughness may be defined as:

$$w_c = \int_0^{(\epsilon_v)_c} \frac{\sigma_{ij}}{\rho} d\epsilon_{ij} \quad (3)$$

where w_c is the critical strain energy density. The value of w_c can be considered as a material property for engineering analyses.

For ductile metals, the material density varies only slightly, even over large deformations. For this reason, it is possible to define an energy per unit volume density as:

$$w_c = \lim_{\Delta V \rightarrow 0} \frac{\Delta W}{\Delta V} \quad (4)$$

$$= \int_0^{\epsilon_v} \sigma_{ij} d\epsilon_{ij} \quad (5)$$

with an associated critical value

$$w_c = \int_0^{(\epsilon_v)_c} \sigma_{ij} d\epsilon_{ij} \quad (6)$$

The energy per unit mass is fundamental, however the energy per unit volume is equally appropriate for constant volume deformation processes.

For the case of an uniaxial stress-strain curve, corresponding to a one-dimensional state of deformation, the critical strain energy density corresponds to the area under the uniaxial stress-strain curve:

$$w_c = \int_0^{\epsilon} \sigma d\epsilon \quad (7)$$

This representation is desirable for use with traditional constitutive formulations which rely on equivalent uniaxial stress-strain curves. In the general case of multiaxial stress and strain, the strain energy density is the sum of the integrals of the individual stress and strain components.

MATERIAL CHARACTERIZATION

In order to obtain an accurate computational simulation of fracture initiation, the constitutive formulation used must be valid for the entire deformation range between zero deformation and fracture initiation. A hybrid computational-experimental procedure is used to determine the constitutive relation for HY1-00 steel [13]. Data from tensile tests performed using cylindrical specimens is used to characterize the material behavior of HY-100 steel. The continuum stress-strain relation determined from the tensile tests is based on the entire range of deformation observed in the ductile material.

This hybrid computational-experimental approach uncouples the influence of test specimen geometry from the observed deformation. This results in a unique scale invariant continuum stress-strain curve. The solution curve for HY-100 steel is shown in Figure 1 and is the stress-strain relation used in the current analysis.

The critical strain energy density as defined by equation (6) or (7) is determined from the solution continuum stress-strain curve, the computationally predicted stress-strain histories at the point of local fracture and the experimentally observed load-displacement point corresponding to tensile specimen fracture. Low and high aspect ratio tensile specimens result in different critical strain energy density values [13]. The low aspect ratio tensile specimens exhibited multiaxial deformation throughout the local stress-strain history. In contrast, the high aspect ratio tensile specimens sustained a predominantly uniaxial state of stress prior to specimen necking followed by a transition to multiaxial stress and strain as the neck develops. The strain energy density at the point of material fracture in the low aspect ratio specimens is used as the critical strain energy density for the current analysis since these specimens are more representative of the multiaxial stress and strain history ahead of the crack tip in the compact specimen. The critical strain energy density coinciding with fracture obtained from the low aspect ratio tensile specimens for HY-100 steel is $882.6 \text{ MN}\cdot\text{m}/\text{m}^3$ ($129,000 \text{ lb}\cdot\text{in}/\text{in}^3$).

FRACTURE INITIATION EXPERIMENT

A compact specimen was used to experimentally determine classical measures of fracture initiation toughness of HY-100 steel. Nominal specimen dimensions, as shown in Figure 2, are $B = 22.9 \text{ mm}$ (0.90 in), $W = 50.8 \text{ mm}$ (2.0 in) and $a/W = 0.5$; where B , W and a are the specimen thickness, width and crack length, respectively. A nominal 2.54 mm (0.10 in) crack measured from the notch tip was produced by fatigue prior to testing. This was accomplished with a servohydraulic testing machine in load control mode with the load cycling between 1.56 and 15.57 kN (350 and 3500 lb). Prior to precracking the alignment of the machine was checked and found to be within 0.0508 mm (0.002 in). After the precrack started to grow the specimen was turned over as necessary to keep the front and back face crack lengths nearly equal. The crack lengths at the front and back face were monitored and measured with traveling microscopes.

An alternating current (AC) electric potential measurement technique was used to determine when crack initiation occurred. The placement of the leads on the specimen are shown in Figure 2. A lock-in amplifier provided a 2 Amp , 5 kHz reference signal to leads A and measured the potential across the crack mouth at leads B.

A series of tests were performed on HY-80 steel to assess the reliability of the AC electric potential method in determining fracture initiation in ductile steels. These tests demonstrated that initiation of crack growth is coincident with attaining a minimum in the measured potential.

The specimen was loaded under displacement control using a servohydraulic test machine at a displacement rate of $7.1 \times 10^{-3} \text{ mm}/\text{sec}$ ($2.8 \times 10^{-4} \text{ in}/\text{sec}$). A microcomputer started the test, performed data acquisition of load and potential across the crack mouth and also controlled a video digitizing board and video camera. The microcomputer acquired data at ten second intervals. For each data set a magnified image of the crack mouth was digitized and displayed on a video monitor. The images were recorded by a video cassette recorder for subsequent measurements of the crack mouth opening displacement (CMOD). As soon as it was realized that the potential reached a minimum the specimen was unloaded, removed from the test machine and marked by heat tinting at 500°F for 90 minutes. The specimen was then cooled in liquid nitrogen, placed in the test machine and rapidly broken. Examination of the tinted surface indicated a negligible amount of crack growth. Post test measurements of the CMOD were performed by manually measuring the distance between the top and bottom corners of the crack mouth of the digitized image with a cursor. The resolution of this technique

was 0.0404 mm (0.0016 in). The instrumentation is shown schematically in Figure 3. The experimentally determined fracture initiation load is 78.06 kN (17,550 lb) and the measured CMOD at fracture initiation is 1.17 mm (0.0459 in).

FRACTURE INITIATION SIMULATION

Fracture initiation in a compact specimen of HY-100 steel is computationally simulated using the ABAQUS finite element code [16] and the concepts described earlier. Nominal test specimen dimensions are used in the computational simulation. The crack in the compact specimen is assumed to have a straight front.

Two and three-dimensional nonlinear analyses were performed. The three-dimensional analysis was performed when results of the two-dimensional analysis indicated that a two-dimensional solution was inadequate to accurately reflect the physically observed deformation.

Two-Dimensional Simulation

The two-dimensional model is shown in Figure 4. A total of 2534 C1D2, CPE8 and CPE8H elements are used to model half of the compact specimen. C1D2 elements are 2-node beam elements used for applying load to the model. CPE8 and CPE8H elements are both 8-node continuum elements with quadratic displacement interpolation. In addition to quadratic displacement interpolation the CPE8H elements incorporate an independently interpolated linear hydrostatic stress [17]. Lagrange multipliers are used to couple the hydrostatic stress to the constitutive relationship. The use of such hybrid elements in regions of large deformation, such as near the crack tip, prevent physically unrealistic nodal displacement constraints from propagating through the mesh. In a model comprised of only nonhybrid elements these unrealistic displacements artificially increase the stiffness for incompressible or nearly incompressible material deformation.

The finite element mesh is more refined in the region surrounding the crack tip than in the remaining portion of the model. Each element along the crack line is 0.4 percent of the total crack length. No crack tip singularity is included in the finite element model.

Fifteen C1D2 beam elements are used to apply load to the compact specimen model. The beam elements are arranged in a finite element model is loaded by application of a point force at the center node of the 'wagon-wheel' loading frame. The beam elements are rigid elastic connectors. Lateral translation of the finite element model is prevented by restraining lateral movement of the center node of the beam element loading frame.

A nonlinear static plane strain analysis was performed using ABAQUS. Both geometric and material nonlinearities are included in the analysis. Geometric nonlinearity is included for accurate evaluation of large strains and rotations which may occur locally prior to failure. Use of Rik's algorithm assures numerical convergence of the finite element solution independent of structural stability. In the modified Rik's algorithm available in ABAQUS, the magnitude of the applied load is an unknown to be determined as part of the solution. The program determines increments of load based on increments of path length along the load-displacement solution curve for the structure. The path length increments are chosen by the program so that a convergent numerical solution is obtained.

The finite element model was subjected to monotonically increasing load until fracture initiation. Fracture initiation occurs when the strain energy density at the crack tip reaches the local material toughness determined from the tensile specimens as described earlier.

The strain energy density profile ahead of the crack tip is shown in Figure 5. The strain energy density is observed to monotonically decrease as the distance from the crack tip increases.

The global load-displacement curves for the two-dimensional finite element model and the experiment are shown in Figure 6. The displacement shown is total CMOD. At low load levels there is good agreement between the experimental and predicted load-displacement curves. However, at approximately 80 percent of the fracture initiation load the experimental results indicate a reduction in stiffness which is not observed in the two-dimensional finite element analysis results. The difference in stiffnesses near fracture initiation is considered to be a result of two-dimensional modeling. Physically occurring out of plane displacements and their effects on the stress and strain state within the compact specimen cannot be accurately modeled by a two-dimensional plane strain analysis.

Three-Dimensional Simulation

A three-dimensional finite element analysis was performed in order to obtain a more accurate solution of the global response of the compact specimen.

The three-dimensional finite element model is shown in Figure 7. Symmetry conditions allow for modeling one-fourth of the actual specimen. A total of 301 elements were used to generate the model. Even though fewer elements are used in the three-dimensional finite element model, the two models require approximately the same amount of computer memory.

The three-dimensional model is made of C3D20 and C3D20H elements. These are 20-node continuum brick elements with quadratic displacement interpolation. In addition to quadratic displacement interpolation the C3D20H elements incorporate an independently interpolated linear hydrostatic stress. As in the two-dimensional analysis, use of such hybrid elements in regions of large deformation prevents artificial stiffening of the finite element model.

The three-dimensional finite element model is considerably less refined than the two-dimensional model. Each element along the crack line is approximately 9.0 percent of the crack length. The three-dimensional model has local refinement at the crack tip and near the outer surface of the compact specimen. There are seven elements across the thickness.

A nonlinear static analysis was performed using ABAQUS. The model was subjected to monotonically increasing displacement until fracture initiation. As in the two-dimensional analysis, geometric and material nonlinearities are included, Rik's algorithm is used to guarantee the numerical convergence of the finite element solution and no crack singularity is included in the finite element model.

The strain energy density profile across the specimen thickness at the plane of the crack is shown in Figure 8. The maximum strain energy density observed in the finite element model occurs at the midplane of the specimen. Therefore, fracture initiation is predicted to begin at the midplane of the specimen. Even though the initial crack front is straight, crack initiation as represented by the strain energy density is nonuniform across the specimen thickness. The shape of the strain energy density profile across the specimen thickness is reminiscent of the curved crack front observed in compact specimens which exhibit ductile tearing as shown in Figure 9. The three-dimensional finite element analysis load-displacement solution is shown in Figure 10.

This three-dimensional finite element model does not have the same degree of refinement in the crack tip region as the two-dimensional finite element model. The lack of refinement in the three-dimensional model requires that the value of strain energy density at the crack tip be extrapolated from the strain energy density a relatively large distance ahead of the crack tip. In order to overcome

this, the strain energy density profile ahead of the crack tip at the midplane of the compact specimen is assumed to be identical to the gradient determined from the two-dimensional plane strain simulation. Then, fracture initiation in the three-dimensional simulation is determined to occur when the curve defined by three-dimensional integration point data along the specimen midplane coincides with the strain energy density profile of the plane strain analysis. The computationally determined fracture initiation load is 78.29 kN (17,600 lb) and the CMOD is 1.18 mm (0.0465 in). The experimentally determined values of fracture initiation load and CMOD are 78.06 kN (17,550 lb) and 1.17 mm (0.0459 in), respectively.

PREDICTION OF FRACTURE TOUGHNESS

Classical fracture parameters are calculated from the load-displacement record and fracture initiation values predicted from the finite element simulation using the concepts discussed previously. The predicted classical fracture parameters are compared with the experimental values.

The apparent stress intensity factor, K , was determined in accordance with ASTM E-399 specifications [18]. While the compact specimen does not allow for the development of plane strain conditions, the specimen can be used to determine the fracture toughness of 22.9 mm (0.90 in) thick sections of HY-100 steel. The predicted K is 134.1 MPa \sqrt{m} (121.7 ksi \sqrt{in}). The experimental value of K is 129.6 MPa \sqrt{m} (117.6 ksi \sqrt{in}). Analytical and experimental values differ by 3.5 percent.

In a similar manner the apparent values of J at fracture initiation were determined from the two load-displacement curves. In accordance with ASTM E-813 procedures [19], J values are based on the load versus load line displacement curves. The predicted fracture initiation J value is 143.7 kJ/m² (820 lb-in/in³). The experimental J value at fracture initiation is 140.2 kJ/m² (800 lb-in/in³). Analytical and experimental values differ by 2.5 percent.

SUMMARY

Fracture toughness at the continuum scale is used as a failure criterion in the current analysis. Material toughness at the continuum scale may be appropriately defined using the strain energy per unit mass at fracture. The continuum stress-strain curve and the associated critical continuum strain energy density are determined from appropriate analysis of observed deformation of simple material tests.

In the current analyses, the continuum response used is determined from cylindrical tensile specimens. An accurate continuum stress-strain curve for large strains which occur prior to fracture is developed from a hybrid computational-experimental procedure. The critical strain energy density associated with fracture is determined from the continuum scale invariant stress-strain curve and the observed point of failure from the cylindrical tensile specimens.

Nonlinear finite element analysis of a compact specimen were performed using the computer code ABAQUS. Good agreement was obtained between experimental and nonlinear two-dimensional finite element load-displacement results to approximately 80 percent of the fracture initiation load. After this point, out of plane displacements reduce the stiffness of the test specimen. A three-dimensional analysis was performed. Nonlinear three-dimensional finite element results duplicate the experimental results for the entire loading history.

Predictions of classical fracture initiation toughness parameters for HY-100 steel agree to within 3.5 percent. This demonstrates that classical fracture measures are not fundamental material parameters. Moreover, these measures may be derived through definition and application of appropriate fundamental concepts and material parameters.

ACKNOWLEDGEMENTS

The authors wish to acknowledge the interest and suggestions of Dr. P. Matic and Mr. P. Father in the computational aspects of the current work.

REFERENCES

1. Rice, J. R., "A Path Independent Integral and the Approximate Analysis of Strain Concentration by Notches and Cracks," *Journal of Applied Mechanics*, Vol. 35, 379-386 (1968).
2. Wells, A. A., "Application of Fracture Mechanics At and Beyond General Yield," British Welding Res. Ass. Report, M13/63 (1963).
3. Dugdale, D. S., "Yielding of Steel Sheets Containing Slits," *Journal of Mechanics of Physics and Solids*, Vol. 8, 100-108 (1960).
4. Hahn, G. T., Sarrate, M., and Rosenfeld, A. R., "Criteria for Crack Extension in Cylindrical Pressure Vessels," *International Journal of Fracture*, Vol. 5, 187-210 (1969).
5. Wang, D. Y. and McCabe, D. E., "Investigation of R-Curve Using Comparative Tests with Center-Cracked Tension and Crack-Line-Wedge-Loaded Specimens," *Mechanics of Crack Growth*, ASTM STP 590, 169-193 (1976).
6. Begley, J. A. and Landes, J. D., "The J-Integral as a Fracture Criterion," *Fracture Mechanics*, ASTM STP 514, 24-39 (1972).
7. Hutchinson, J. W. and Paris, P. C., "The Theory of Stability Analysis of J-Controlled Crack Growth," *Elastic-Plastic Fracture*, ASTM STP 668, 37-64 (1977).
8. McMeeking, R. M. and Parks, D. M., "On Criteria for J. Dominance of Crack-Tip Fields in Large Scale Yielding," *Elastic Plastic Fracture*, ASTM STP 668, 175-194 (1977).
9. Clark, W. G., Jr., "Some Problems in the Application of Fracture Mechanics," *Fracture Mechanics: 13th Conference*, ASTM STP 743, 269-287 (1981).
10. Jolles, M. I., Matic, P., Kirby, G. C. III, Gensheimer, V. M. and Harvey, D. P. II, "Critical Issues and Directions for Fracture Mechanics and Structural Integrity," NRL Memo. Rpt. 6035 (1988).
11. Freudenthal, A. M., *The Inelastic Behavior of Engineering Materials and Structures*, 1950.
12. Gillemot, L. F., "Criterion of Crack Initiation and Spreading," *Engineering Fracture Mechanics*, Vol. 8, 239-253 (1976).
13. Matic, P., Kirby, G. C. III, and Jolles, M. I., "The Relationship of Tensile Size and Geometry Effects to Unique Constitutive Parameters for Ductile Materials," NRL Memo. Rpt. 5936 (1987).
14. Matic, P. and Jolles, M. I., "Defects, Constitutive Behavior and Continuum Toughness Considerations for Weld Integrity Analysis," NRL Memo. Rpt. 5935, 1987.

15. Matic, P. and Jolles, M. I., "The Influence of Weld Metal Properties, Weld Geometry and Applied Load on Weld System Performance," NRL Memo. Rpt. 5987 (1987).
16. Hibbitt, H. D., Karlsson, B. I., and Sorensen, E. P., *ABAQUS User's Manual* (1984).
17. Hibbitt, H. D., Karlsson, B. I., and Sorensen, E. P., *ABAQUS Theory Manual* (1984).
18. "Standard Test Method for Plane Strain Fracture Toughness of Metallic Materials," E 399-83, *Annual Book of ASTM Standards, Section 3*, 519-554 (1984).
19. "Standard Test Method for JIC, A Measure of Fracture Toughness," E 813-81, *Annual Book of ASTM Standard, Section 3*, 763-781 (1984).

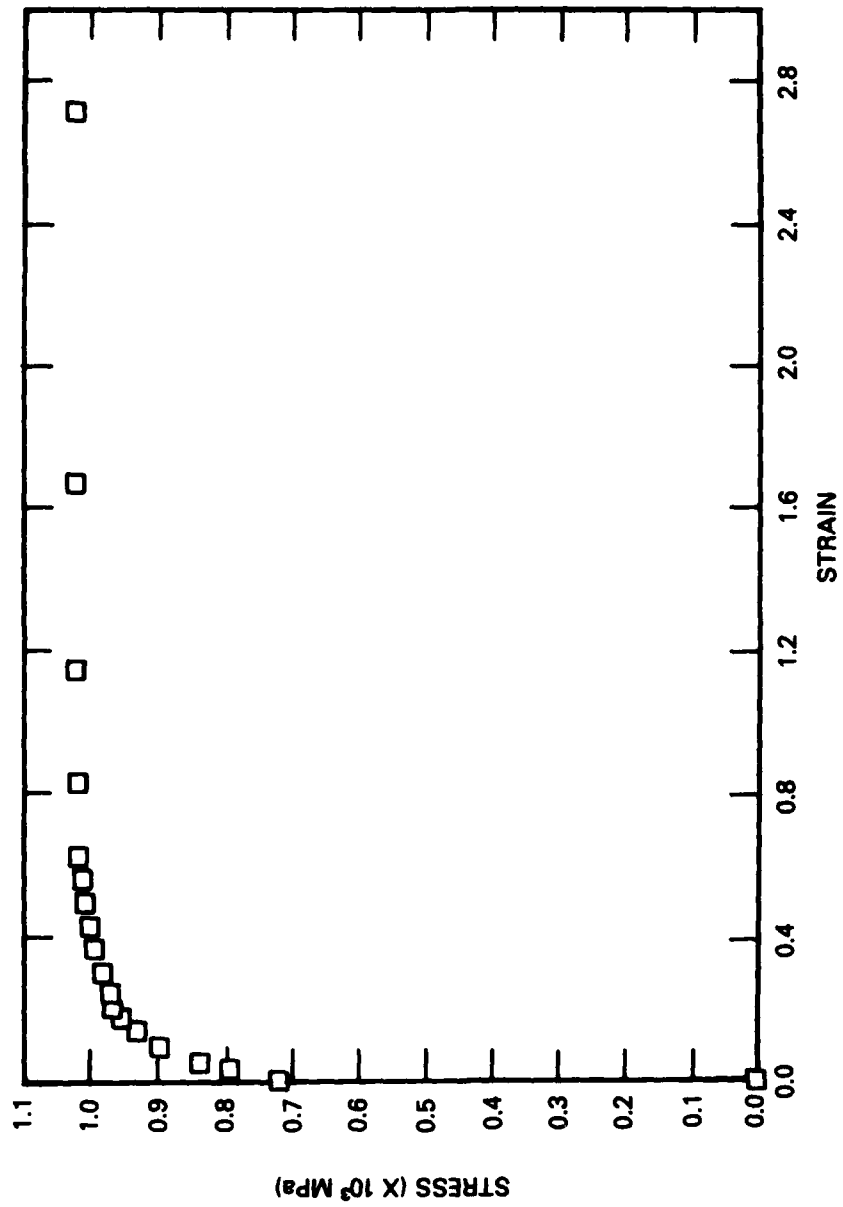


Fig. 1 — Continuum Stress-Strain Solution Curve for HY-100

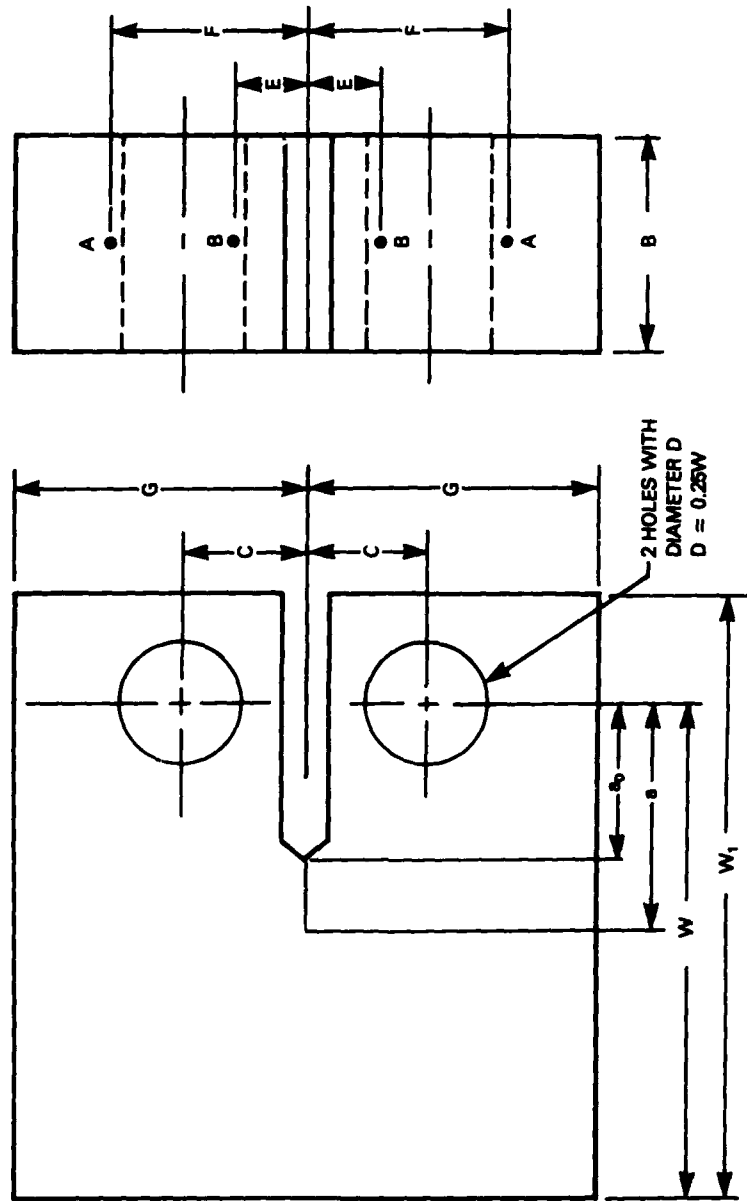


Fig. 2 — Compact Specimen Geometry and AC Potential Lead Locations

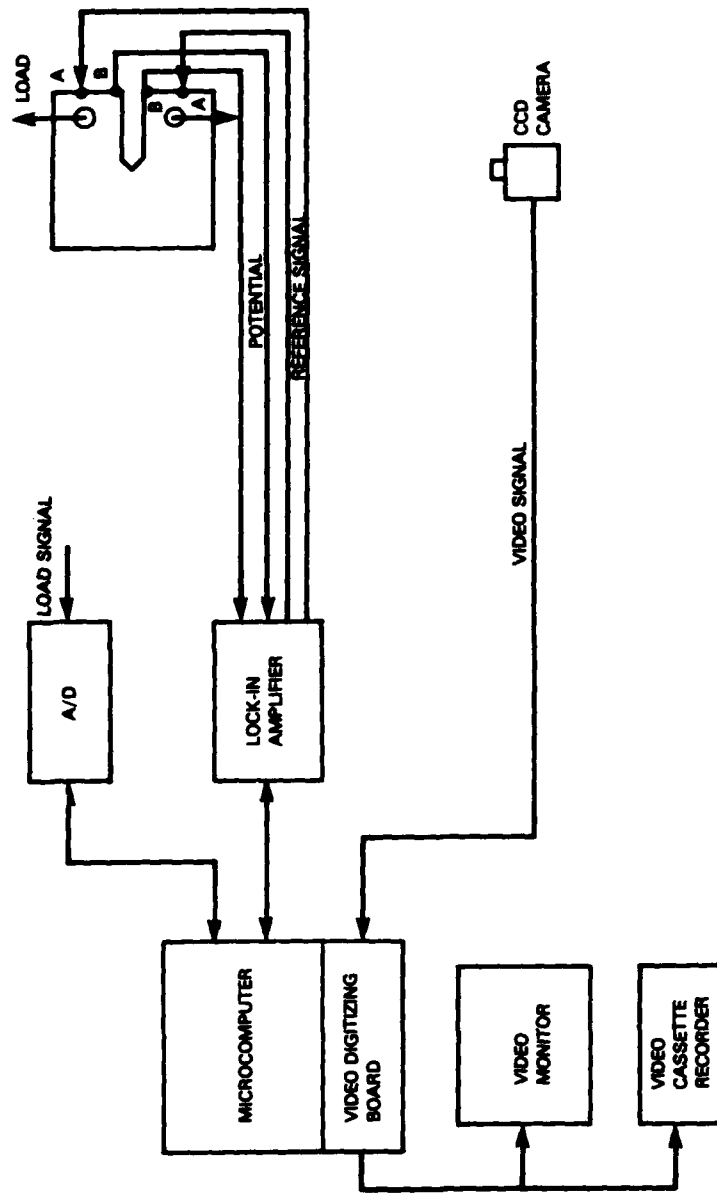


Fig. 3 -- Instrumentation for Fracture Initiation Experiments

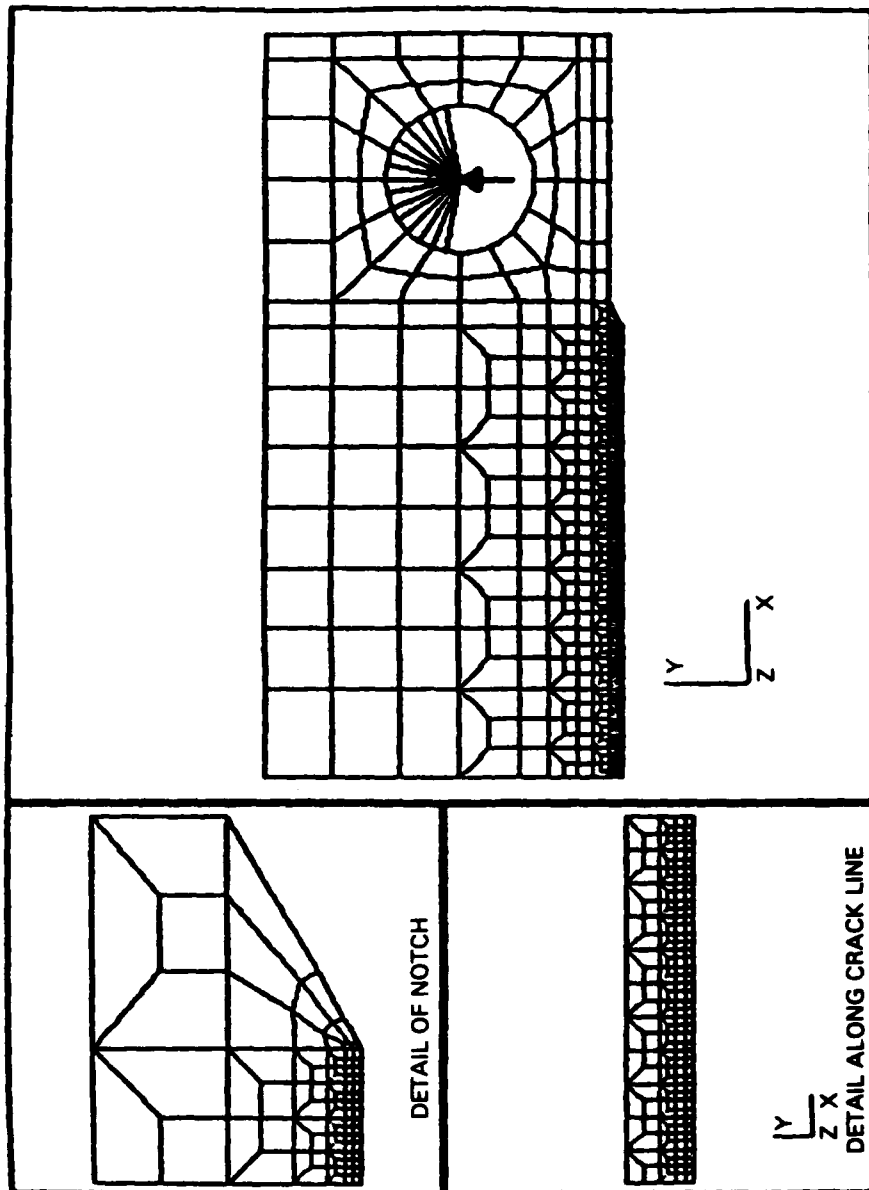


Fig. 4 — Two-Dimensional Finite Element Model

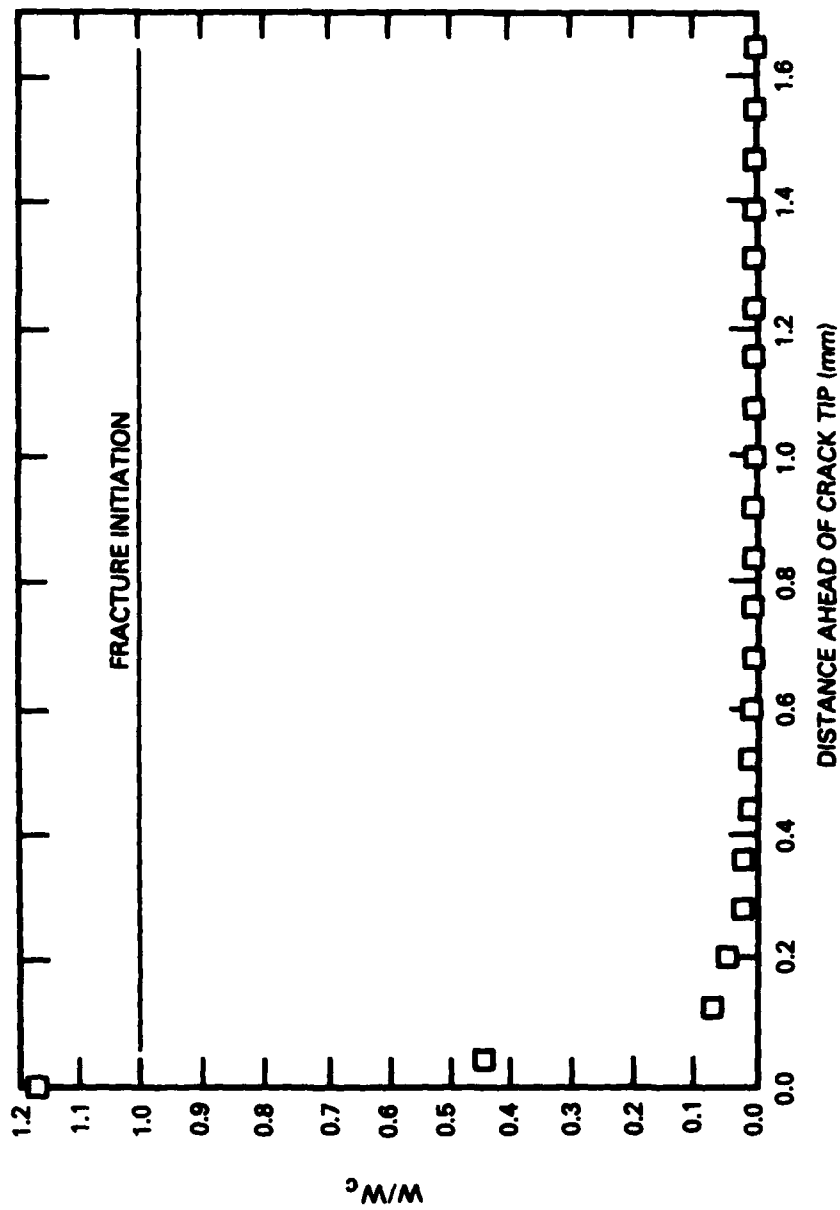


Fig. 5 — Normalized Strain Energy Density Ahead of the Crack Tip (Plane Strain)

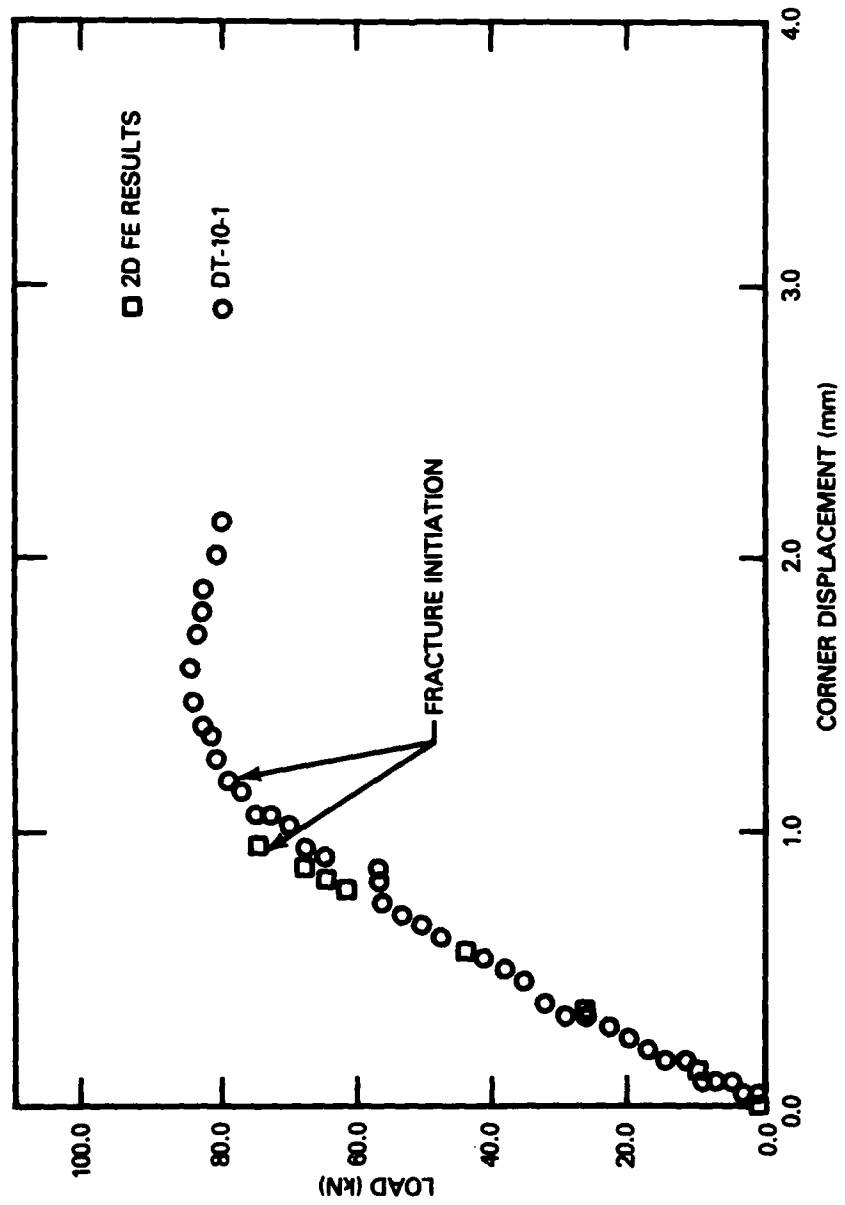


Fig. 6 — Load-Displacement Results Showing Two-Dimensional (Plane Strain) Finite Element Results

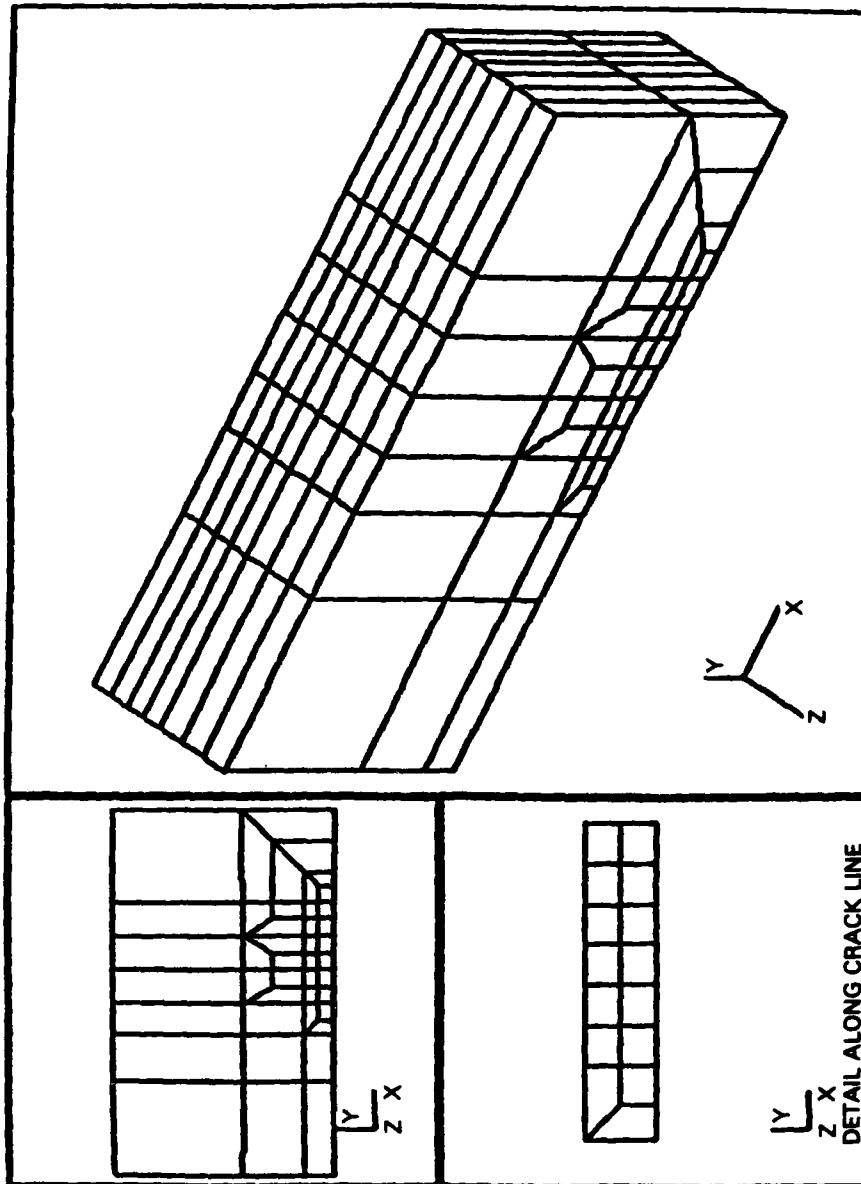


Fig. 7 — Three-Dimensional Finite Element Model

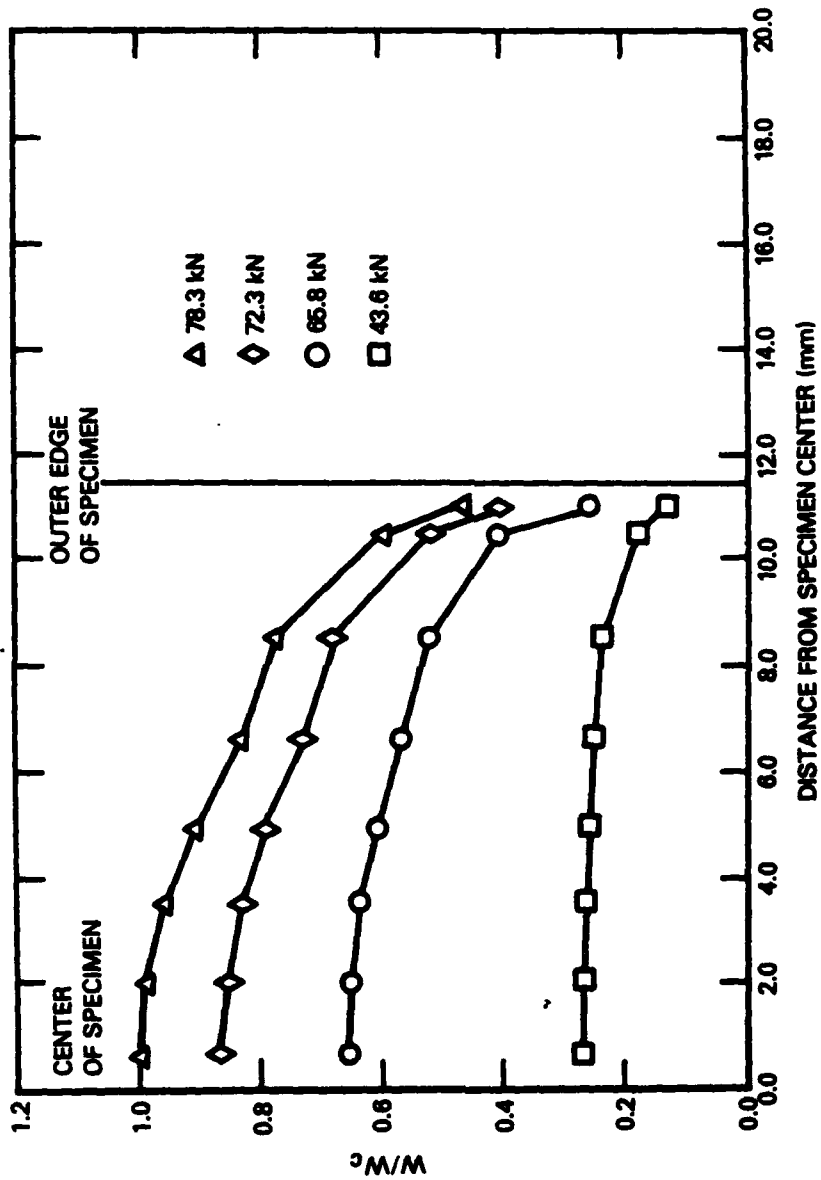


Fig. 8 — Variation in Normalized Strain Energy Density Across the Specimen Thickness

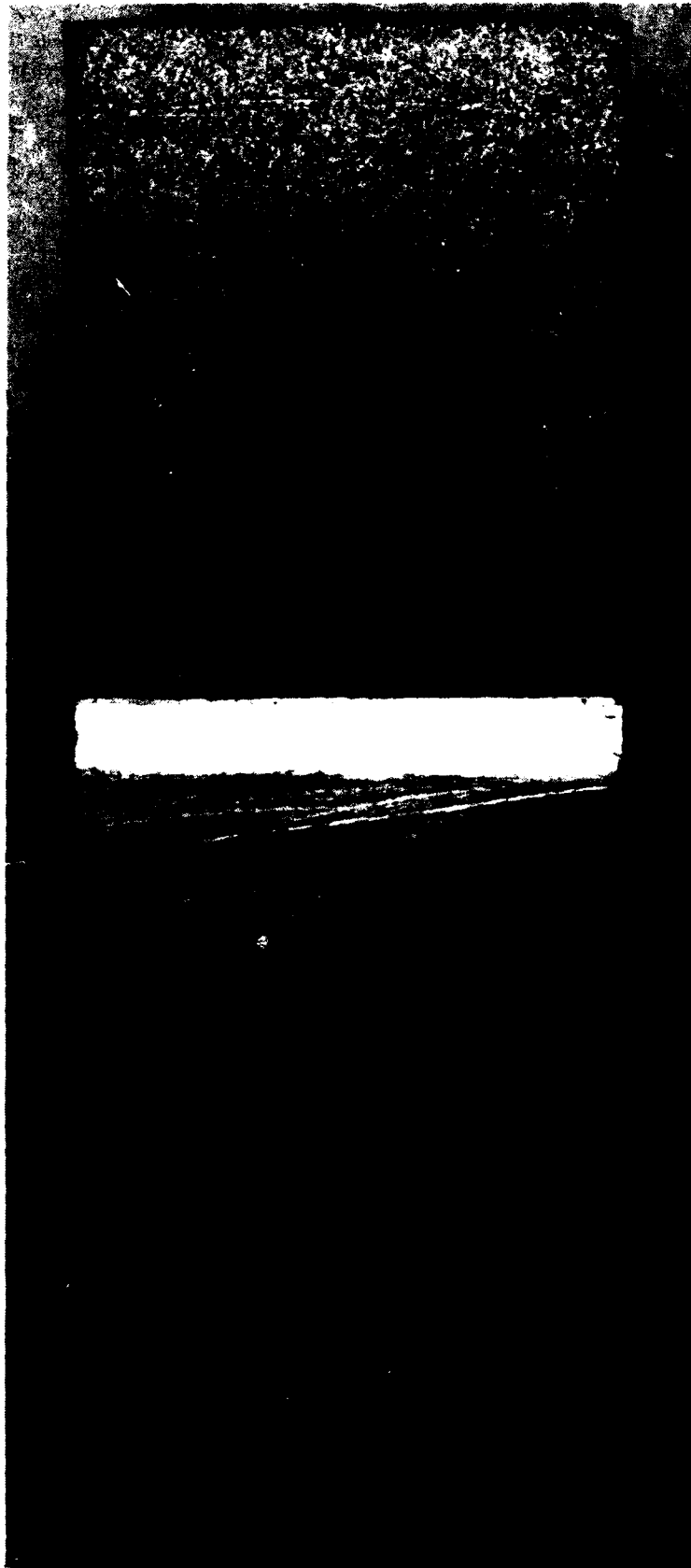


Fig. 9 — Compact Specimen Showing Curved Crack Front

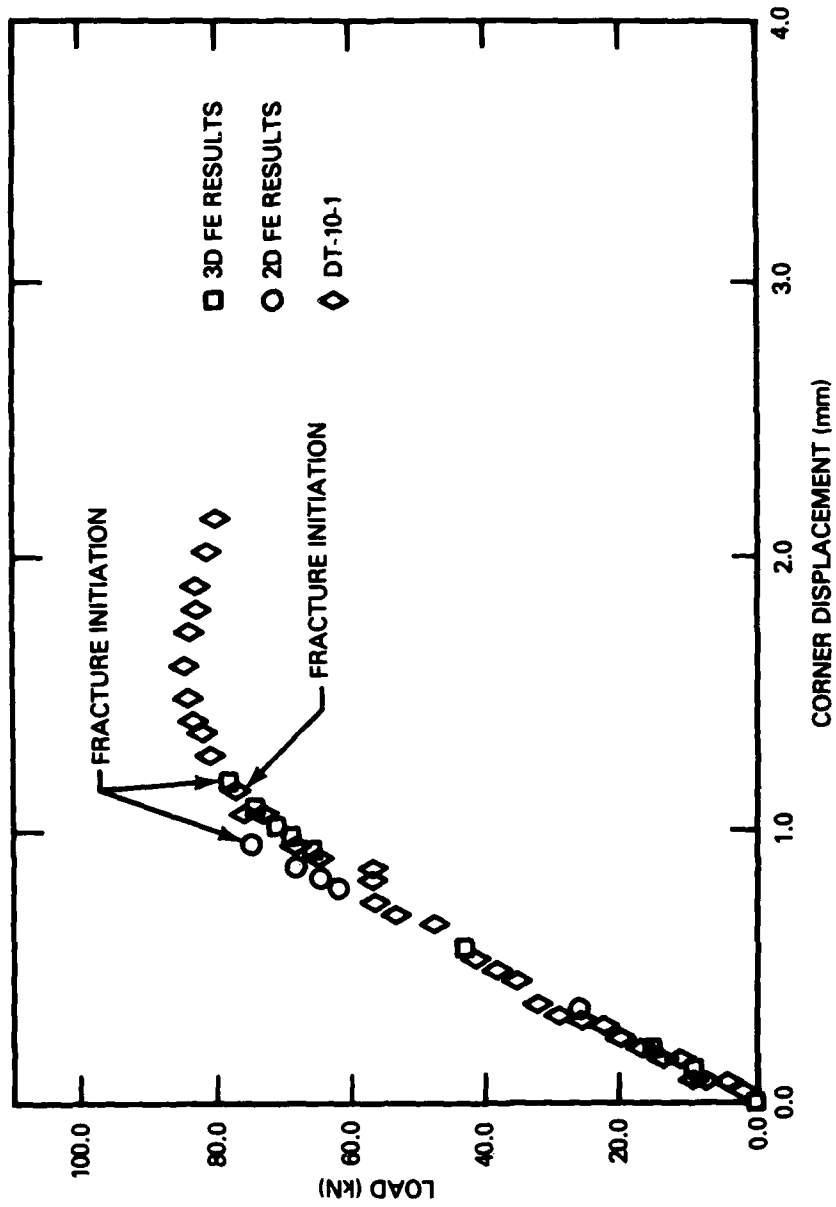


Fig. 10 -- Load-Displacement Results Showing Two-Dimensional (Plane Strain) and Three-Dimensional Finite Element Results